Journal of the European Ceramic Society 39 (2019) 4625–4633

Contents lists available at ScienceDirect

Journal of the European Ceramic Society

journal homepage: www.elsevier.com/locate/jeurceramsoc

Original Article

Fabrication and mechanical properties of carbon fibers/lithium aluminosilicate ceramic matrix composites reinforced by in-situ growth SiC nanowires

Chi Wang[a], Long Xia[a,*], Bo Zhong[a], Hua Yang[b], Longnan Huang[a], Li Xiong[a], Xiaoxiao Huang[c], Guangwu Wen[d]

[a] School of Materials Science and Engineering, Harbin Institute of Technology (Weihai), Weihai, 264209, PR China
[b] School of Science, Lanzhou University of Technology, Lanzhou, 730050, PR China
[c] School of Materials Science and Engineering, Harbin Institute of Technology, Harbin, 150001, PR China
[d] School of Materials Science and Engineering, Shandong University of Technology, Zibo, 255049, Shandong, PR China

ARTICLE INFO

Keywords:
Multi-scaled reinforcements
SiC nanowires
Carbon fiber
Lithium aluminosilicate glass ceramic
Ceramic matrix composites

ABSTRACT

To improve the mechanical properties of carbon fibers/lithium aluminosilicate (C_f/LAS) composites, C_f/LAS with in-situ grown SiC nanowires (SiC_{nw}-C_f/LAS) were prepared by chemical vapor phase reaction, precursor impregnation, and hot press sintering, consecutively. The effect of multi-scaled reinforcements (micro-scaled C_f and nano-scaled SiC_{nw}) on the mechanical properties was investigated. The phase composition, microstructure and fracture surface of the composites were characterized by XRD, Raman Spectrum, SEM, and TEM. The morphology of SiC_{nw} has a close relation with the content of Si. Microstructure analysis suggests that the growth of SiC nanowires depends on the VLS mechanism. The multi-scale reinforcement formed by C_f and SiC_{nw} can significantly improve the mechanical properties of C_f/LAS. The bending strength of SiC_{nw}-C_f/LAS reaches to 597 MPa, achieving an increase of 19% to C_f/LAS. Moreover, the samples show a maximum fracture toughness of 11.01 MPa $m^{1/2}$, achieving an increase of 46.4% to C_f/LAS. Through analysis of the fracture surface, the improved mechanical properties could be attributed to the multi-scaled reinforcements by the pull-out and debonding of C_f and SiC_{nw} from the composites.

1. Introduction

Lithium aluminosilicate (LAS) is a kind of glass-ceramic materials, which possesses excellent chemical durability, high-temperature stability, low coefficient of thermal expansion and thermal shock resistance [1–5]. LAS has been considered as a functional and structural material in many industrial applications, such as high-temperature heat insulation systems, aerospace structures, and optical lens [6,7].

Nevertheless, some problems still exist for wide applications for LAS. Generally, LAS glass ceramics are fabricated through the precipitation of β-spodumene or β-eucryptite from the glass matrix which demonstrates relatively low mechanical properties. Their flexural strength and fracture toughness are roughly located in the range of 100–250 MPa and 1–1.5 MPa $m^{1/2}$, respectively [8], which hardly meets the application needs of structural materials. To enhance the mechanical properties of LAS is still a challenge, the introduction of reinforcements has become a popular method to improve the mechanical properties of LAS. Currently, for LAS and other ceramic matrix composites (CMC), reinforcements generally use metal particles [9,10], carbon fibers [11,12], alumina fibers [13], PVA fibers [14], zinc oxide nanowires [15], carbon nanotubes [16,17], graphene [18]. Regardless of the composition and shape, the reinforcements could be generally divided into two types, micro-scale, and nano-scale reinforcements, based on the differences in dimensions. Though the CMC with a single reinforcement is widely studied and applied, the reports on CMC with multiple reinforcements are still rare. Particularly, researches on CMC with multi-scale reinforcement are preliminary. The multi-scale reinforcements have more advantages than the single reinforcement, such as higher mechanical properties and more functional properties [19–23].

Compared with other reinforcements, carbon fiber (C_f) possesses the outstanding advantages of high strength, low density and excellent wear resistance for structural application [24]. According to reported studies, the fracture toughness and work of fracture of C_f/LAS

* Corresponding author.
E-mail address: xialonghit@gmail.com (L. Xia).

https://doi.org/10.1016/j.jeurceramsoc.2019.06.035
Received 30 November 2018; Received in revised form 15 June 2019; Accepted 17 June 2019
Available online 19 June 2019
0955-2219/

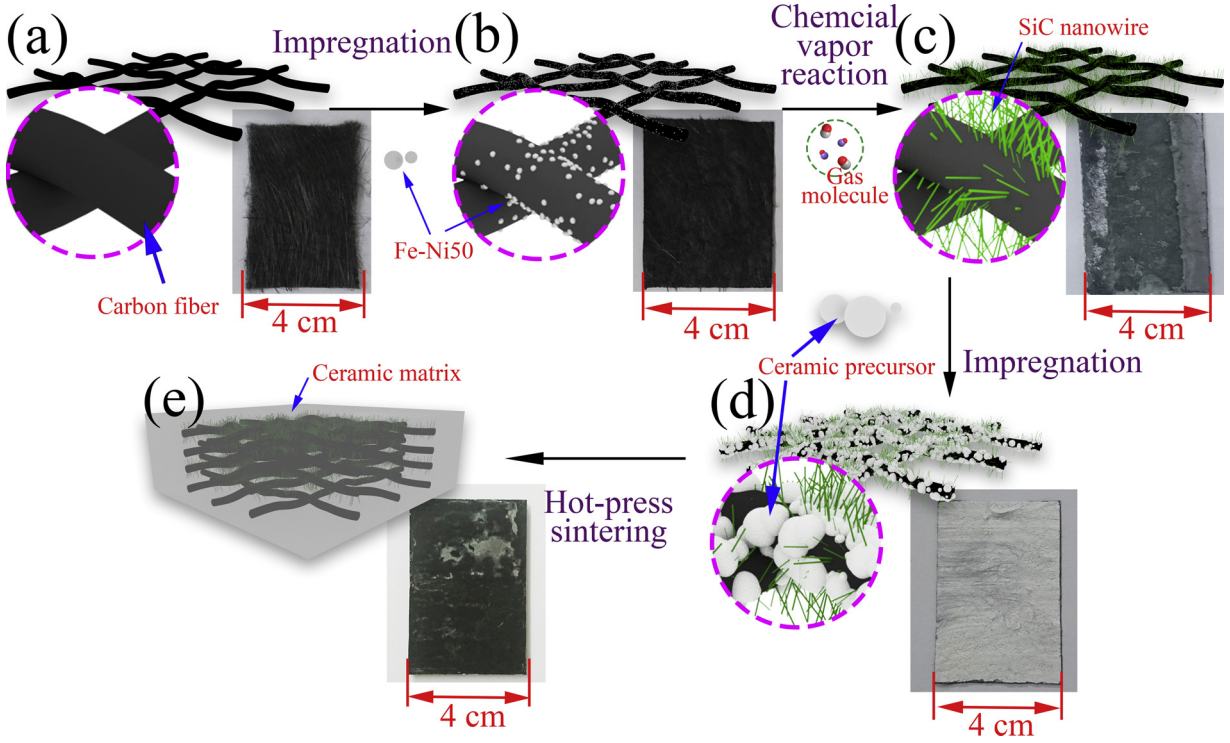

Fig. 1. Schematic illustration of composites preparation.

composites could reach 11.4 MPa $m^{1/2}$ and 12 kJ·m^{-2}. Herein, to further enhance the mechanical properties, nano-scale SiC is introduced into C_f/LAS to achieve multi-scale reinforcement. SiC_{nw} could be regarded as an effective reinforcement, due to the excellent mechanical properties and chemical stability [25,26]. Some studies about SiC_{nw} as a kind of reinforcement in ceramic matrix composite were reported [25,27]. Here, we report multi-scaled reinforcement of C_f and SiC nanowire (SiC_{nw}-C_f) fabricated by the chemical vapor reaction process, and the SiC_{nw}-C_f/LAS was fabricated by precursor impregnation and hot-pressing sintering. The effects of the multi-scaled reinforcements (micro-scaled C_f and nano-scaled SiC_{nw}) on the mechanical properties were systematically investigated as well.

2. Experimental

2.1. materials and fabrication

Fig. 1 shows the schematic illustration for the fabrication of specimens. First, the C powder (Acetylene Black, Jinghong New Energy Industries, China) and Fe-Ni50 powder (1200 mesh, Changsha Tianjiu Metal Co. Ltd., China), as a raw material and catalyst, were dispersed in a dilute PVA solution and stirred ultrasonically for 0.5 h. The PAN-based non-woven C_f felts (Jiangsu Tianniao High Technology Co. Ltd., China) were impregnated with this solution and dried for 24 h in 80 ℃. During the growing process of nanowires, the C_f felts were suspended over the ball-milled Si powder (2000 mesh, Liaoning Nitrogen compound Co. Ltd., China) under an argon atmosphere at 1500 ℃ for 4 h.

LAS sol in the form of β-spodumene (Li_2O-Al_2O_3-$4SiO_2$) was synthesized following a sol-gel method by starting with mixing boehmite sol, silica sol and the lithium salt, using deionized water as media. The slurry was prepared with the LAS sol through ball milling approach [28–31].

The C_f felts, and the SiC_{nw}-C_f felts were stacked and infiltrated into the as-prepared slurry of LAS. SiC_{nw}-C_f/LAS were prepared by hot-pressing with 10 MPa at 1300 ℃ for 0.5 h under vacuum condition.

To investigative the effect of SiC_{nw}, the mole ratio between Si and C was designed as 1:1, 1:2 and 1:3 during the growth of SiC_{nw}. The SiC_{nw}-C_f samples were respectively referred to as SiC_{nw}-C_f-1, SiC_{nw}-C_f-2, and SiC_{nw}-C_f-3. The composites with different SiC_{nw}-C_f were respectively referred to as SiC_{nw}-C_f/LAS-1, SiC_{nw}-C_f/LAS-2, and SiC_{nw}-C_f/LAS-3. For the comparison, the composite without SiC_{nw} was prepared in the same process, referred to as C_f/LAS.

2.2. Characterization

The flexural strength and fracture toughness were tested by a mechanical testing machine (Instron 3345, Norwood, MA, UK) to investigate the effect of the in-situ grown SiC_{nw} on the mechanical properties of LAS. The flexural curve was measured by three-point-bending tests on 3 mm × 4 mm × 36 mm bars with a span of 30 mm and a cross-head speed of 0.5 mm/min. Single-edge-notched-beam (SENB) test was used to assess the fracture toughness with a cross-head of 0.05 mm/min and a span of 20 mm. The samples were 2 mm × 4 mm × 20 mm with a notch depth to sample thickness ratio of 0.5. For each test, at least five specimens were used to obtain the mean value.

The phase of the samples was characterized by XRD (DX-2700, Dandong Haoyuan) with Cu Ka radiation and Raman Spectrum. The morphology of in-situ grown SiC_{nw} and fracture surfaces were observed by FE-SEM (MERLIN Compact, Zeiss) and TEM (JEOL-2100, Hitachi, Ltd.).

3. Results and discussion

3.1. Phase analysis and microstructure of SiC_{nw}-C_f

Fig. 1 shows the photograph of the samples at different stages of fabrications. As shown in Fig. 1c, the fiber felts exhibit green colored surface for all samples, consistent with other reports of SiC_{nw} growth [32,33].

Fig. 2a shows X-ray diffraction patterns for SiC_{nw}-C_f samples and C_f. The diffraction peak at 25.9° is observed in all of the diffraction

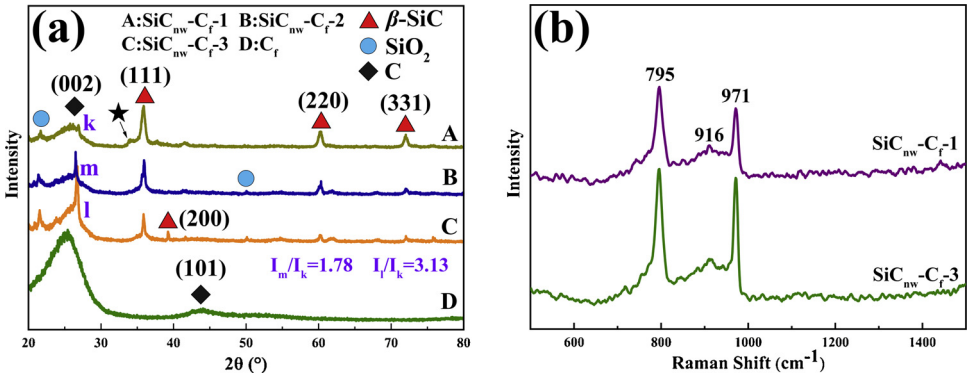

Fig. 2. X-ray diffraction patterns and Raman Spectra of SiC_{nw}-C_f and C_f.

patterns, which is assigned to (002) diffraction plane of C_f. SiC is characterized by the four diffraction peaks, which are indexed into (1 1 1), (2 0 0), (2 2 0), and (3 1 1) diffraction planes of SiC. Meanwhile, the shoulder (33.6° peak marked by a star) emerges on the left side of the (1 1 1) peak. The similar phenomenon in SiC_{nw} preparation is also observed by other researchers, which can be ascribed to the stacking faults formed during the growth of SiC_{nw} [32,34,35]. Compared with carbon fiber felt, the intensity of (0 0 2) diffraction peak of carbon was further improved as shown in Fig. 2a, which is recognized as the product of graphitization of excess carbon at high temperatures. The relative intensities of (0 0 2) diffraction peak of specimens are also listed in Fig. 2a. As the relative content of carbon increases, the intensity of the diffraction peak increases. Also, the diffraction peak of SiO_2 is observed in the XRD patterns, which results from a small amount of remaining oxygen in the argon atmosphere.

Fig. 2b shows the Raman Spectra of SiC_{nw}-C_f. The peaks of 795 cm^{-1} and 971 cm^{-1} corresponding to SiC appear in the Raman Spectra. Compared to the peaks of the SiC block, the peaks of SiC_{nw}-C_f have a small redshift, due to the comprehensive results of quantum confinement effect and internal defects [36,37]. The peak of 916 cm^{-1} is indexed as SiO_2, which is consistent with XRD results.

Fig. 3 shows the microstructures of the surface of SiC_{nw}-C_f-1. SiC_{nw} are synthesized in a considerable amount on the surface of C_f. As shown in high magnification image (Fig. 3c and d), most of SiC_{nw} are straight and long. Particular attention is paid to the surface of C_f, and it is found that SiC_{nw} are rooted in the surface of C_f (Fig. 3d).

FE-SEM images of the composites are shown in Fig. 4. The morphology of SiC_{nw} has a close relation with the Si:C ratio. The nanowires in SiC_{nw}-C_f-1 (Fig. 4a) are straight, and irregular nanowires appear in SiC_{nw}-C_f-2 (Fig. 4b). Conspicuously, the content of irregular nanowires in SiC_{nw}-C_f-3 (Fig. 4c) increases.

3.2. The growth mechanism of SiC_{nw}

The FE-SEM and TEM were applied to characterize the structure and mechanism of growth of SiC_{nw}. As shown in Fig. 5a, b, and c, the SiC_{nw} exhibits a clean surface and uneven diameter along the length direction. The screw-like shape boundary of SiC_{nw} could be attributed to the stacking faults of SiC_{nw}, which is consistent with XRD and Raman Spectra results. The interplanar spacing for SiC crystals is 0.25 nm in Fig. 5d, which corresponds to the (1 1 1) interplanar spacing of β-SiC crystal [38,39]. The corresponding selected area electron diffraction (SAED) patterns are shown in Fig. 5e, f, and g, which reveal stacking faults in the crystal. The formation of stacking faults is quite common in SiC nanostructures [34,40]. Meanwhile, the metallic ball at the top of SiC_{nw} is observed in Fig. 5a and b. It can be concluded that the

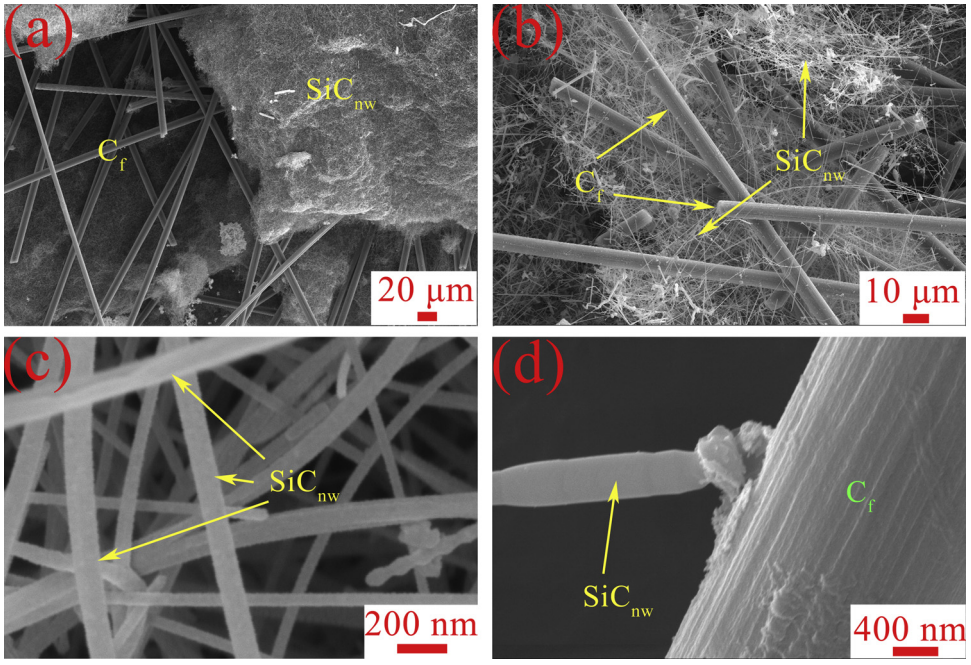

Fig. 3. FE-SEM images of SiC_{nw}-C_f-1: (a), (b) low magnification; (c), (d) high magnification.

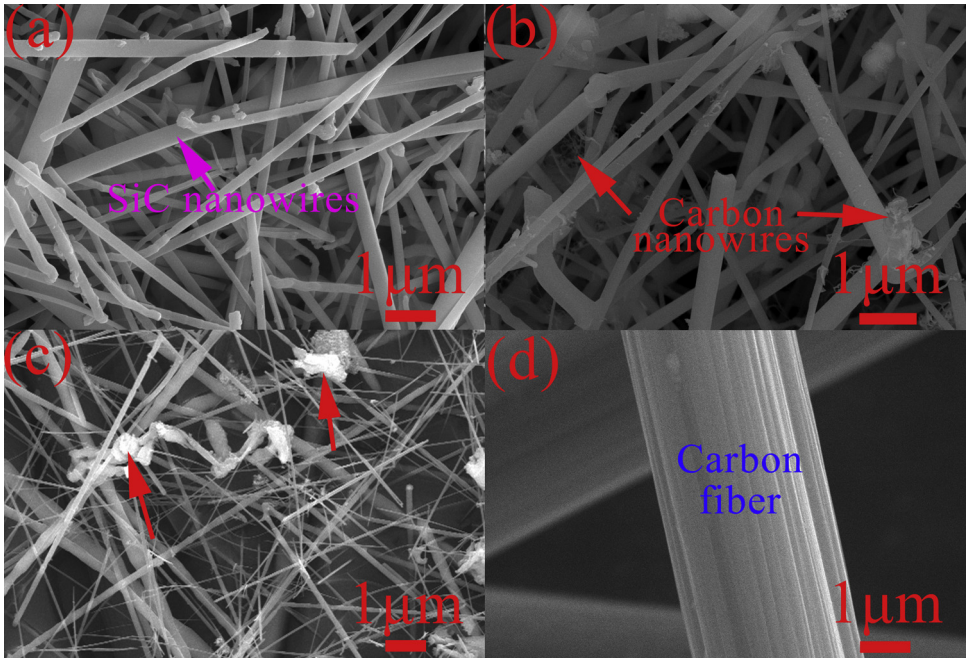

Fig. 4. FE-SEM images of (a) SiC_{nw}-C_f-1; (b) SiC_{nw}-C_f-2; (c) SiC_{nw}-C_f-3; (d) C_f.

microstructure of SiC_{nw} implies typical VLS growth mechanism [38,41].

As shown in Fig. 6, Fe-Ni50 alloy melts into liquid droplets on the surface of C_f at high temperature. Meanwhile, residual oxygen in the Argon atmosphere reacts with Si and C to produce SiO and CO, as shown in the following chemical reactions:

$$2Si(s) + O_2(g) = 2SiO(g) \quad (1)$$

$$2C(s) + O_2(g) = 2CO(g) \quad (2)$$

The SiO and CO molecules would preferentially adsorb at the surface of liquid catalyst and broken of chemical bonding occurs due to the presence of catalyst. The carbon atoms and silicon atoms move toward the inside of the droplet, leading to the formation of Fe-Ni-Si-C alloy, and the oxygen atoms react with carbon monoxide to form carbon dioxide, which overflow from the surface of the droplet. The reaction equation is as follows:

$$SiO(g) + 3CO(g) = Si(atom) + C(atom) + 2CO_2(g) \quad (3)$$

Since the vapor is continuously supplied by an overpressure of SiO and CO, the Si and C would eventually supersaturate in the droplet, which will precipitate in the form of eutectic at nucleation point, such as interface between liquid droplet and solid [42]. After nucleation, C

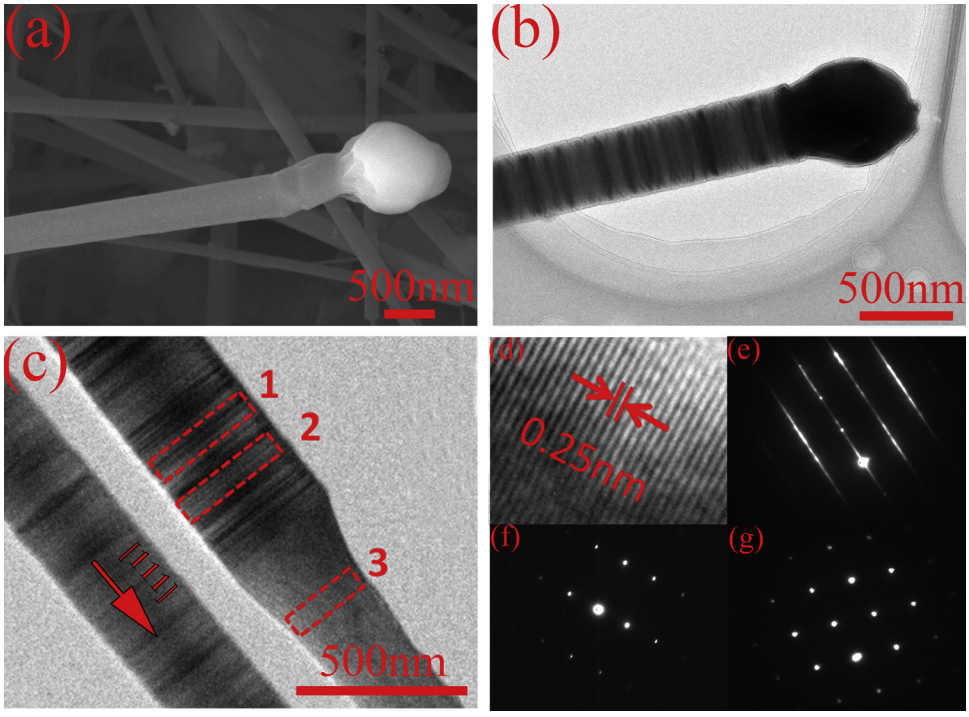

Fig. 5. (a) FE-SEM images of SiC_{nw}; (b), (c), (d) TEM images of SiC_{nw}; (e), (f), (g) SAED pattern of region 1, 2, 3 in.(c) respectively.

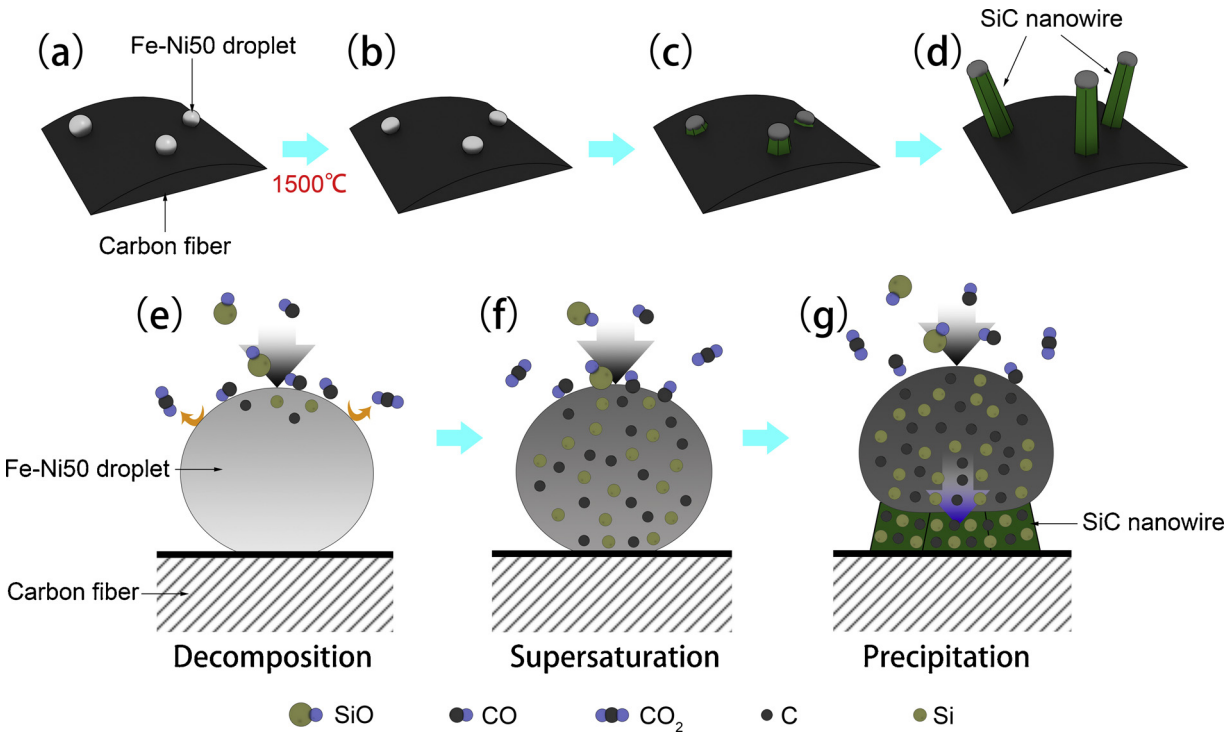

Fig. 6. Schematic of the in-situ SiC_{nw} growth mechanism.

and Si dissolution and SiC crystal precipitates continuously at the liquid-solid interface, and then the nanowires form. It has been confirmed that the (1 1 1) crystal planes possess the largest planar spacing and the lowest specific surface energy direction. Hence, SiC crystal mainly precipitates along the [1 1 1] direction and grows into nanowires [32].

While the above process is being carried out, the carbon dioxide reacts with the carbon powder to form carbon monoxide, and the reaction is as follows:

$$CO_2(g) + C(s) = 2CO(g) \quad (4)$$

This process can supply the carbon monoxide consumed in the reaction. The reaction for the whole process is as follows:

$$Si(s) + C(s) = SiC(s) \quad (5)$$

Stacking faults is one of most common defects in single crystal preparation, which could reduce the surface energy of SiC surface and benefit the axial growth [38]. This conclusion is also supported by the TEM and XRD results.

Irregular nanowires were analyzed by SEM, EDS and TEM, and the results are shown in Fig. 7. The elemental composition of the two points of the irregular nanowire of SiC_{nw}-C_f-3 is shown in Fig. 7b, and it is found that the main composition of the irregular nanowires is carbon, and a small amount of silicon. In the TEM image, one straight nanowire is wrapped in the irregular nanowire, is identified as silicon carbide. The interplanar spacing of the crystals in the outer nanowires is about 0.337 nm, and the orientations of the grains are clearly not the same. The length is the same as the (0 0 2) crystal plane of graphite, indicating that the outer layer is composed of microcrystalline graphite, confirming the results of XRD. This microcrystalline graphite is produced by graphitization of excess carbon at high temperatures.

Fig. 8 shows the SEM image of SiC_{nw}-C_f-2. The relative content and diameter of irregular nanowires are less than SiC_{nw}-C_f-3, which indicates that the yield of nanowires composed of graphite crystallites is relatively low. As shown in Fig. 8c, the surface of the silicon carbide nanowires is uneven compared to SiC_{nw}-C_f-1, due to the adhesion of microcrystalline carbon to the surface. Since the relative content of carbon in this ratio is small compared to SiC_{nw}-C_f-3, microcrystalline graphite does not completely wrap the SiC_{nw}.

3.3. Mechanical properties

As shown in Fig. 9, the SiC_{nw}-C_f/LAS-1 shows the highest bending strength and fracture toughness. The bending strength of SiC_{nw}-C_f/LAS-1 reaches to 597 ± 36 MPa, which means an increase of 19% compared with C_f/LAS. Fracture toughness also increase separately by 46.4%, reaching 11.01 MPa $m^{1/2}$. This result demonstrates that the in-situ growth SiC_{nw} has a significant effect on the mechanical properties of SiC_{nw}-C_f/LAS.

The Fig. 10 shows the bending stress-strain curves for different composites. The C_f/LAS sample exhibited brittle fracture, consistent with previous studies that some ceramic-based materials have no toughness even when carbon fibers are added [31,43,44]. In the reported studies [45], at high temperatures, atoms in the ceramic matrix, especially lithium atoms, diffuse into the fibers. Li_2O reacts with the carbon of surface of the fibers, which affects the surface graphitic basal planes of the carbon fibers.

$$C(s) + Li_2O(s) = CO(g) + 2Li(s) \quad (6)$$

The atoms diffuse more quickly into the carbon fiber due to the irreversible damage of the surface of carbon fibers. This process has a negative impact on the performance of carbon fiber. Meanwhile, at high temperatures, lithium atoms react with carbon atoms to generate graphite intercalation compounds (GIC), which causes the crack to deflect in the axial direction and propagate.

$$Li(s) + 24C(s) = LiC_{24}(s) \quad (7)$$

However, the generation of GIC has a great relationship with temperature. The yield of GIC is maximized at 1400 °C and the yield at 1350 °C is very low. In the present study, the sintering temperature is 1300 °C, it is difficult to generate GIC. In summary, the combined effect of these two processes always results in damage to the surface of the carbon fiber, making it easier for the carbon fiber to break radially during crack propagation. The fracture process is macroscopically

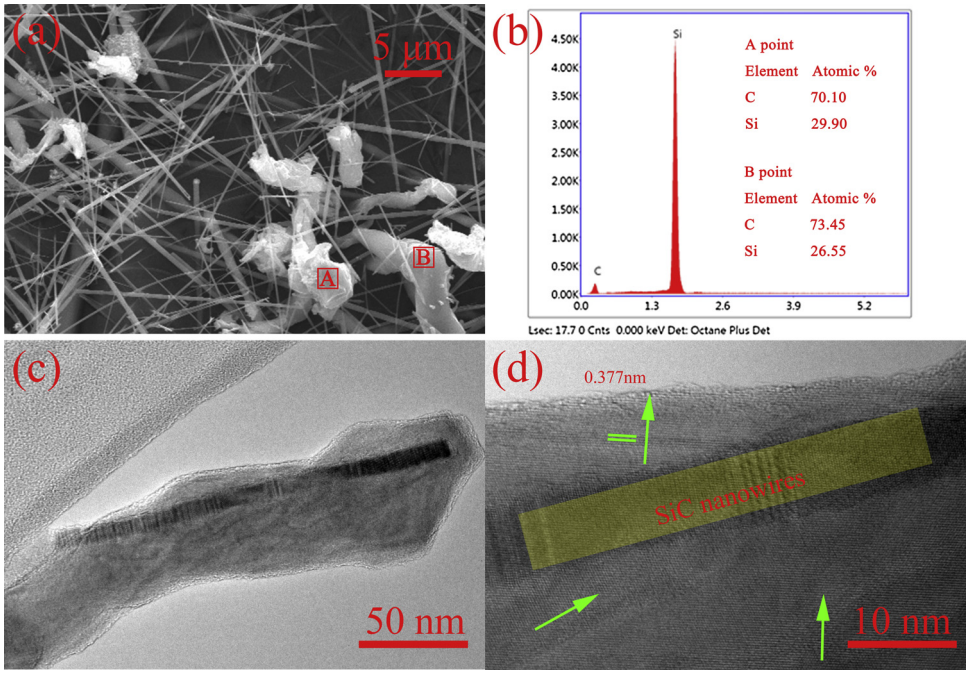

Fig. 7. FE-SEM image, EDS results, TEM image and HRTEM image of SiC_{nw}-C_f-3.

characterized by brittle fracture.

SiC_{nw}-C_f/LAS-2 and SiC_{nw}-C_f/LAS-3 also exhibit brittle fracture characteristics. Notably, the stress-strain curve for SiC_{nw}-C_f/LAS-1 shows a sawtooth shape on the top, suggesting a pseudo-plastic fracture behavior. This phenomenon illustrates that the toughness of composites is improved by the introduction of SiC_{nw}.

3.4. Fracture surfaces

To understand the reinforcement mechanism of LAS by SiC_{nw}, the fracture surfaces of the sample were observed by FE-SEM. Fig. 11 shows the morphology of the fracture surface of SiC_{nw}-C_f/LAS-1 after the flexural test. In Fig. 11a and b, the fracture surface of SiC_{nw}-C_f/LAS-1 is characterized by a porous structure accompanying with the fiber pull-out (as indicated by yellow arrows). This phenomenon often occurs in the fracture of fiber-reinforced ceramic material composites [46,47].

The high-resolution images of the fracture surface are obtained to investigative the effect of SiC_{nw}. The nanowires are imbedded in the matrix, as Fig. 11c, which shows that the nanowires are well combined with the matrix during the fabrication of the composite. Meanwhile, the debonding and pull-out of SiC nanowires are observed in Fig. 11d, e, and f.

Fig. 12 shows the schematic of the cracking process of the composite. Similar to fiber-reinforced ceramic matrix composites, the addition of SiC nanowires could increase the composite toughness, which mainly contains pull-out and debonding of SiC_{nw}, and crack deflection. The nanowires embedded in the ceramic matrix form a network structure as shown in Fig. 11d. Under a specific load, initial cracks are generated, propagate in the matrix and meet with SiC_{nw} network. Due to the high

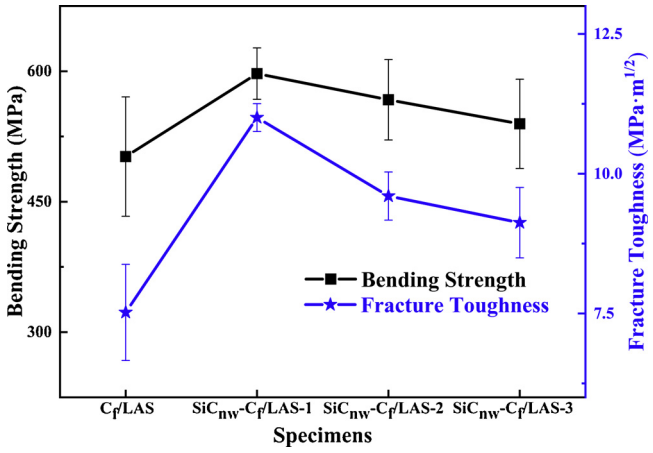

Fig. 9. The bending strength and fracture toughness of composites.

strength of SiC nanowire, cracks would bypass the nanowires. More tortuous or branch paths are created during the propagation process of cracks to dissipate or disperse energy (Fig. 12d), which helps increase the fracture toughness. In the other hand, when the crack is opened to both sides, the energy is dissipated by the interfacial friction in the interface between the SiC_{nw} and ceramic matrix during debonding or pulling-out of nanowires. Thus, the fracture toughness is improved (Fig. 12f). Even if the nanowire breaks during the debonding or pull-out process, the fracture energy can be absorbed to enhance the fracture toughness of the composite. Compared to C_f in micro-scale (Fig. 12f), the strengthening effect of SiC_{nw} belongs to nano-scale, which acts on

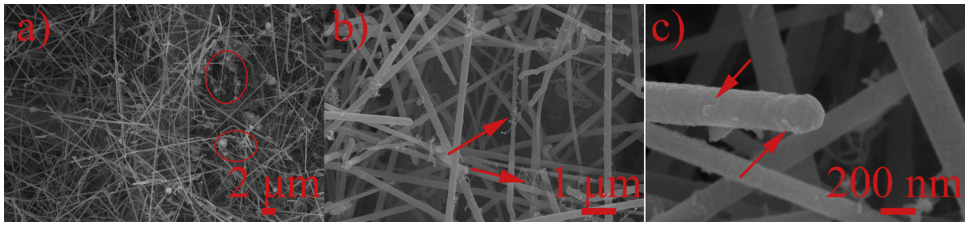

Fig. 8. FE-SEM images of SiC_{nw}-C_f-2.

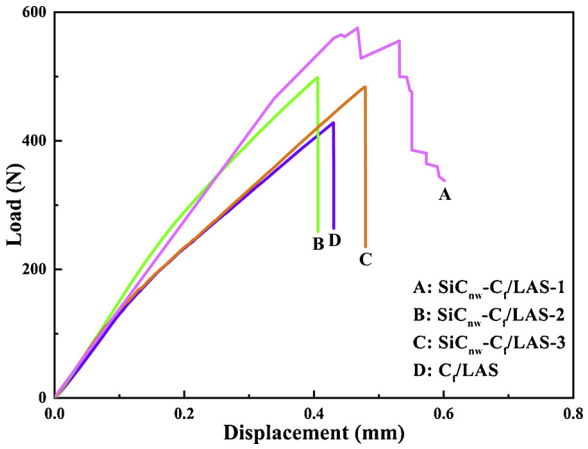

Fig. 10. The bending stress-strain curves for specimens.

smaller crack propagation and prevents tinier cracks from expanding effectively.

When varying the Si:C ratio during the SiC_{nw} preparation, the mechanical properties of the resulting composites are altered. Compared with SiC_{nw}-C_f/LAS-1, SiC_{nw} in SiC_{nw}-C_f/LAS-2 and in SiC_{nw}-C_f/LAS-3 contain carbon nanowires as by-products obtained during growth. The carbon nanowires have poor mechanical properties because they are composed of microcrystalline graphite. The carbon nanowires in the composite not only do not have reinforcement effect, but also generate more cracks even before applying any load. This conclusion is also supported by the bending strength and fracture toughness of composites. As the carbon nanowires amount increases, the mechanical properties of the composite material decrease.

In summary, the SiC_{nw} could serve as the an effectively second reinforcement, constructing multi-scaled reinforcement with C_f, which is beneficial for the improvement of mechanical properties. The reinforcing mechanical for SiC_{nw}-C_f/LAS could be attributed to the pull-out and debonding of C_f and SiC_{nw} and crack deflection.

4. Conclusions

This paper reports a study of the preparation and characterization of SiC_{nw}-C_f/LAS composites. The SiC_{nw}-C_f was firstly fabricated by the chemical vapor reaction process through the VLS mechanism, and the SiC_{nw}-C_f/LAS composites were fabricated by precursor impregnation and hot-pressing. The bending strength and fracture toughness of SiC_{nw}-C_f/LAS are higher than C_f/LAS. The addition of SiC_{nw} results in increases by 19% and 46.4% in bending strength (597 ± 36 MPa) and fracture toughness (11.01 ± 0.36 MPa·m$^{1/2}$), respectively. Through analysis of the fracture surface, the improved mechanical properties could be attributed the multi-scaled reinforcements by the pull-out and debonding of C_f and SiC_{nw} from the composites and crack propagation.

Acknowledgements

This work was supported by the National Natural Science

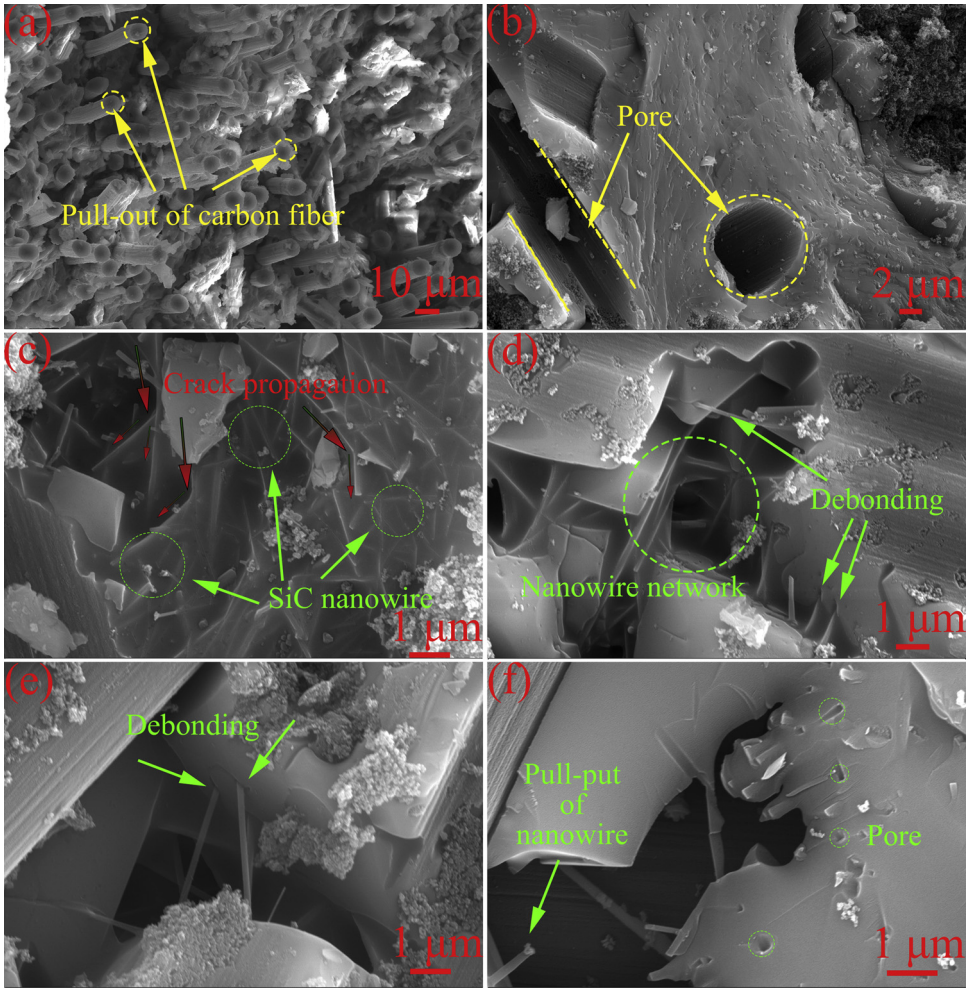

Fig. 11. FE-SEM images of fracture surfaces of the SiC_{nw}-C_f/LAS-1 composite: (a), (b): low resolution; (c)-(f): high resolution.

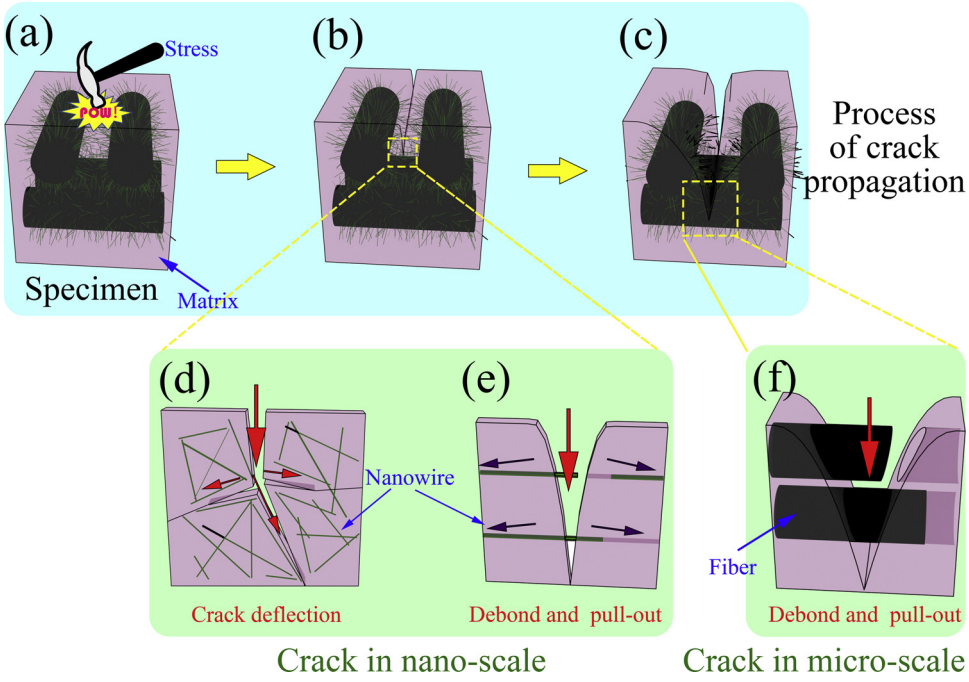

Fig. 12. Schematic of the cracking process of composite.

Foundation of China (Grant No. 51621091, 51872058, 51772060 and 51302050), Key Laboratory of Advanced Structural-Functional Integration Materials & Green Manufacturing Technology, Harbin Institute of Technology, Harbin, 150001, China.

References

[1] S. Barbi, P. Miselli, C. Siligardi, Failure analysis of glazed LAS glass-ceramic containing cerium oxide, Ceram. Int. 43 (1) (2017) 1472–1478.
[2] D. Feng, Y. Zhu, F. Li, Z. Li, Influence investigation of CaF2 on the LAS based glass-ceramics and the glass-ceramic/diamond composites, J. Eur. Ceram. Soc. 36 (10) (2016) 2579–2585.
[3] A.M. Hu, K.M. Liang, F. Zhou, G.L. Wang, F. Peng, Phase transformations of Li2O–Al2O3–SiO2 glasses with CeO2 addition, Ceram. Int. 31 (1) (2005) 11–14.
[4] K. Łączka, K. Cholewa-Kowalska, M. Środa, J. Rysz, M.M. Marzec, M. Łączka, Glass–ceramics of LAS (Li2O–Al2O3–SiO2) system enhanced by ion-exchange in KNO3 salt bath, J. Non. Solids 428 (2015) 90–97.
[5] Y. Yang, L. Xia, T. Zhang, B. Shi, L. Huang, B. Zhong, X. Zhang, H. Wang, J. Zhang, G. Wen, Fe3O4@LAS/RGO composites with a multiple transmission-absorption mechanism and enhanced electromagnetic wave absorption performance, Chem. Eng. J. 352 (2018) 510–518.
[6] L. Xia, F. Jin, T. Zhang, X. Hu, S. Wu, G. Wen, Enhanced oxidation resistance of carbon fiber reinforced lithium aluminosilicate composites by boron doping, Corros. Sci. 99 (2015) 240–248.
[7] L. Xia, X. Wang, G. Wen, B. Zhong, L. Song, Nearly zero thermal expansion of β-spodumene glass ceramics prepared by sol–gel and hot pressing method, Ceram. Int. 38 (6) (2012) 5315–5318.
[8] L. Xia, G.W. Wen, C.L. Qin, X.Y. Wang, L. Song, Mechanical and thermal expansion properties of β-eucryptite prepared by sol–gel methods and hot pressing, Mater. Des. 32 (5) (2011) 2526–2531.
[9] S.I. Durowaye, O.I. Sekunowo, A.I. Lawal, O.E. Ojo, Development and characterisation of iron millscale particle reinforced ceramic matrix composite, J. Taibah Univ. Sci. 11 (4) (2017) 634–644.
[10] R.-R. Enrique, A.R.-G. José, E.-V. Sergio, C.-S. Brianda, E.-G. Ivanovich, M.-S. Roberto, Effect of particle size and titanium content on the fracture toughness of particle-ceramic composites, Mater. Today Proc. 3 (2) (2016) 249–257.
[11] S. Tang, C. Hu, Design, preparation and properties of carbon Fiber reinforced ultra-high temperature ceramic composites for aerospace applications: a review, J. Mater. Sci. Technol. 33 (2) (2017) 117–130.
[12] L. Longbiao, Effects of loading type, temperature and oxidation on mechanical hysteresis behavior of carbon fiber-reinforced ceramic-matrix composites, Eng. Fract. Mech. 169 (2017) 336–353.
[13] S. Poges, C. Monteleone, K. Petroski, G. Richards, S.L. Suib, Preparation and characterization of an oxide-oxide continuous fiber reinforced ceramic matrix composite with a zinc oxide interphase, Ceram. Int. 43 (18) (2017) 17121–17127.
[14] J. Qiu, X.N. Lim, E.-H. Yang, Fatigue-induced in-situ strength deterioration of micro-polyvinyl alcohol (PVA) fiber in cement matrix, Cem. Concr. Compos. 82 (2017) 128–136.
[15] L. Zhang, W. Jiao, Preparation and performance of ZnO nanowires modified carbon fibers reinforced NiFe2O4 ceramic matrix composite, J. Alloys Compd. 581 (2013) 11–15.
[16] J.-H. Shin, J. Choi, M. Kim, S.-H. Hong, Comparative study on carbon nanotube- and reduced graphene oxide-reinforced alumina ceramic composites, Ceram. Int. 44 (7) (2018) 8350–8357.
[17] O. Tapasztó, H. Lemmel, M. Markó, K. Balázsi, C. Balázsi, L. Tapasztó, The influence of sintering on the dispersion of carbon nanotubes in ceramic matrix composites, Chem. Phys. Lett. 614 (2014) 148–150.
[18] P. Miranzo, M. Belmonte, M.I. Osendi, From bulk to cellular structures: a review on ceramic/graphene filler composites, J. Eur. Ceram. Soc. 37 (12) (2017) 3649–3672.
[19] X. Yang, Z. Wang, M. Xu, R. Zhao, X. Liu, Dramatic mechanical and thermal increments of thermoplastic composites by multi-scale synergetic reinforcement: carbon fiber and graphene nanoplatelet, Mater. Des. 44 (2013) 74–80.
[20] L. Ma, L. Wu, X. Cheng, D. Zhuo, Z. Weng, R. Wang, Improving the interlaminar properties of polymer composites using a situ accumulation method to construct the multi-scale reinforcement of carbon nanofibers/carbon fibers, Compos. Part A Appl. Sci. Manuf. 72 (2015) 65–74.
[21] X. Du, T. Gao, Z. Qian, Y. Wu, X. Liu, The in-situ synthesis and strengthening mechanism of the multi-scale SiC particles in Al-Si-C alloys, J. Alloys Compd. (2018).
[22] M.J. Palmeri, K.W. Putz, T. Ramanathan, L.C. Brinson, Multi-scale reinforcement of CFRPs using carbon nanofibers, Compos. Sci. Technol. 71 (2) (2011) 79–86.
[23] G. Mittal, K.Y. Rhee, V. Mišković-Stanković, D. Hui, Reinforcements in multi-scale polymer composites: processing, properties, and applications, Compos. Part B Eng. 138 (2018) 122–139.
[24] K. Jian, Z.-H. Chen, Q.-S. Ma, H.-f. Hu, W.-W. Zheng, Effects of polycarbosilane infiltration processes on the microstructure and mechanical properties of 3D-Cf/SiC composites, Ceram. Int. 33 (6) (2007) 905–909.
[25] J. Prakash, P.S. Sarkar, J. Bahadur, K. Dasgupta, Effect of in-situ grown SiC nanowire and dense SiC on oxidation resistance of carbon fiber/SiC nanowire/SiC matrix composite in high temperature atmospheric environment, Corros. Sci. 135 (2018) 46–56.
[26] J. Chen, L. Ding, L. Xin, F. Zeng, J. Chen, Thermochemistry and growth mechanism of SiC nanowires, J. Solid State Chem. 253 (2017) 282–286.
[27] Y. Guo, L. Zhang, H. Li, S. He, X. Tian, H. Sheng, Q. Song, Microstructure and interlaminar shear property of carbon fiber-SiC nanowire/pyrolytic carbon composites with SiC nanowires growing at different positions, Ceram. Int. 44 (10) (2018) 11448–11455.
[28] L. Xia, G. Wen, L. Song, X. Wang, The crystallization behavior and thermal expansion properties of β-eucryptite prepared by sol–gel route, Mater. Chem. Phys. 119 (3) (2010) 495–498.
[29] L. Xia, G.-w. Wen, L. Song, X.-y. Wang, The effect of aluminum sources on synthesis of low expansion glass–ceramics in lithia–alumina–silica system by sol–gel route, J. Non. Solids 355 (48-49) (2009) 2349–2354.
[30] L. Xia, X. Wang, G. Wen, X. Li, C. Qin, L. Song, Influence of brick pattern interface structure on mechanical properties of continuous carbon fiber reinforced lithium aluminosilicate glass–ceramics matrix composites, J. Eur. Ceram. Soc. 32 (2) (2012) 409–418.
[31] L. Xia, B. Zhong, T. Song, S. Wu, T. Zhang, G. Wen, Reactive hot pressing and mechanical properties of B 4 C/Li 2 O–Al 2 O 3 –SiO 2 composites, J. Non. Solids 432 (2016) 510–518.

[32] J. Li, J. Sha, J. Dai, Z. Lv, J. Shao, S. Wang, Z. Zhang, Fabrication and characterization of carbon-bonded carbon fiber composites with in-situ grown SiC nanowires, Carbon 118 (2017) 148–155.
[33] J. Li, Y. Zhang, Y. Kong, L. Hu, C. Jin, Z. Xi, Synthesis, characterization and field emission properties of SiC nanowires prepared by chemical vapor reaction, Vacuum 146 (2017) 87–92.
[34] Y. Liu, J. Men, W. Feng, L. Cheng, L. Zhang, Catalyst-free growth of SiC nanowires in a porous graphite substrate by low pressure chemical vapor infiltration, Ceram. Int. 40 (8) (2014) 11889–11897.
[35] Y. Zhang, Y. Zhang, J. Han, Y. Zhou, L. Hu, W. Yao, W. Qu, The effect of annealing temperature on micro-structure and mechanical properties of C/SiC composites, Mater. Sci. Eng. A 497 (1-2) (2008) 383–387.
[36] W. Dai, J.H. Yu, Y. Wang, Y.Z. Song, H. Bai, N. Jiang, Single crystalline 3C–SiC nanowires grown on the diamond surface with the assistance of graphene, J. Cryst. Growth 420 (2015) 6–10.
[37] X. Qiang, H. Li, Y. Zhang, S. Tian, J. Wei, Synthesis and Raman scattering of SiC nanowires decorated with SiC polycrystalline nanoparticles, Mater. Lett. 107 (2013) 315–317.
[38] J. Men, Y. Liu, R. Luo, W. Li, L. Cheng, L. Zhang, Growth of SiC nanowires by low pressure chemical vapor infiltration using different catalysts, J. Eur. Ceram. Soc. 36 (15) (2016) 3615–3625.
[39] R. Wu, Z. Yang, M. Fu, K. Zhou, In-situ growth of SiC nanowire arrays on carbon fibers and their microwave absorption properties, J. Alloys Compd. 687 (2016) 833–838.
[40] J.X. Dai, J.J. Sha, Z.F. Zhang, Y.C. Wang, W. Krenkel, Synthesis of high crystalline beta SiC nanowires on a large scale without catalyst, Ceram. Int. 41 (8) (2015) 9637–9641.
[41] X. Li, G. Zhang, R. Tronstad, O. Ostrovski, Synthesis of SiC whiskers by VLS and VS process, Ceram. Int. 42 (5) (2016) 5668–5676.
[42] J.-J. Niu, J.-N. Wang, A study in the growth mechanism of silicon nanowires with or without metal catalyst, Mater. Lett. 62 (4-5) (2008) 767–771.
[43] F. He, Y. Liu, Z. Tian, C. Zhang, F. Ye, L. Cheng, L. Zhang, Carbon fiber/SiC composites modified SiC nanowires with improved strength and toughness, Mater. Sci. Eng. A 734 (2018) 374–384.
[44] L. Xia, C. Wang, D. Feng, K. Wang, H. Han, T. Zhang, G. Wen, Enhanced mechanical properties of carbon fibre/lithium aluminosilicate composites modified by SiB6 addition, Adv. Appl. Ceram. 117 (8) (2018) 500–509.
[45] L. Xia, G.L. Zhao, X.X. Huang, G.W. Wen, J.Q. Dai, Z.H. Zhao, Effect of graphite intercalation compounds in the interfacial zone on the mechanical and thermal properties of unidirectional carbon fiber reinforced spodumene composite, Acta Mater. 61 (9) (2013) 3522–3532.
[46] N. Ranjbar, S. Talebian, M. Mehrali, C. Kuenzel, H.S. Cornelis Metselaar, M.Z. Jumaat, Mechanisms of interfacial bond in steel and polypropylene fiber reinforced geopolymer composites, Compos. Sci. Technol. 122 (2016) 73–81.
[47] V. Fiore, T. Scalici, G. Di Bella, A. Valenza, A review on basalt fibre and its composites, Compos. Part B Eng. 74 (2015) 74–94.